

# Simulating inputs of parvalbumin inhibitory interneurons onto excitatory pyramidal cells in piriform cortex

**Jeffrey E. Dahlen**  
*jdahlen@ucsd.edu*

and

**Kerin K. Higa**  
*khiga@ucsd.edu*

Department of Neuroscience  
University of California San Diego  
La Jolla, CA 92093

## Abstract

The balance of excitation and inhibition within most sensory cortices is co-tuned to a given stimulus. However, unlike other sensory cortices, it has been reported from in vivo recordings that widespread global inhibition governs sparse stimulus-evoked excitation in the piriform cortex. Further in vitro physiology has demonstrated that this global inhibition is achieved through local activation of feed-back inhibition by layer 3 (L3) interneurons, which make perisomatic synapses onto pyramidal cells. L3 interneurons are composed of two major classes of GABA-releasing inhibitory interneurons found in all sensory cortices: somatostatin (SOM) and parvalbumin (PV) expressing neurons. Both SOM and PV neurons have been well characterized as significant contributors to cortical inhibitory networks, yet their functional roles within local circuits remain unknown. Here we attempt to model this circuit using minimum Hodgkin-Huxley type models. First, we adapted previously defined models of thalamic and cortical SOM, PV and pyramidal neurons to fit physiology data recorded from piriform cortex SOM, PV and pyramidal neurons. We then used experimentally derived glutamate and GABA synaptic coupling coefficients to create our neural feedback circuit. We aimed to create simplistic models of these neurons which would describe the relative latencies of inhibition each cell type would contribute onto pyramidal cells.

## 1 Introduction

### 1.1 Background Neuroscience

Sensory processing begins through integration of signals received from sensory neurons in the peripheral nervous system, which is then transmitted to the brain for processing. “Processing” of these signals occurs in sensory cortical networks, which are comprised primarily of two types of cells: excitatory principle neurons and inhibitory interneurons. In most sensory cortices, excitatory input from sensory neurons leads to activation of similar populations of excitatory and inhibitory neurons.

In the olfactory bulb, specific odorant molecules bind to their respective olfactory sensory neurons, which then project afferents and propagate these signals to the main olfactory bulb (MOB), where a majority of odor identification takes place (Figure 1). Mitral and tufted cells from the MOB then project axons via the lateral olfactory tract (LOT) to the primary olfactory (piriform) cortex, where odor perception is believed to occur. Unlike other sensory cortices, where excitation and inhibition are balanced for a given stimuli, previous work has shown widespread inhibition to be a staple of the piriform cortex [1].

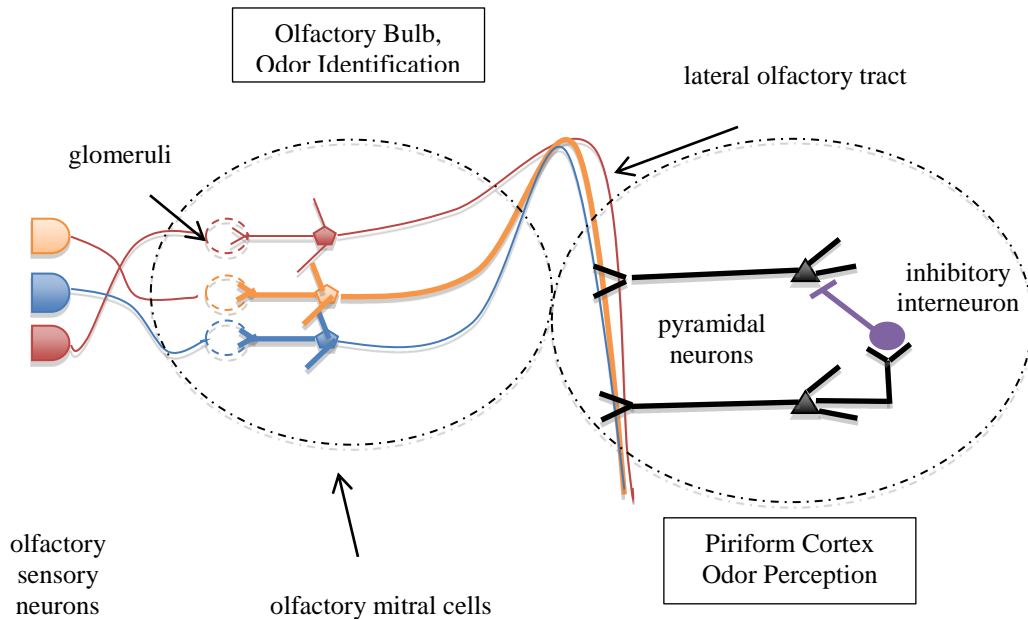


Figure 1: Diagram of olfaction from olfactory sensory neurons to the piriform cortex.

## 1.2 Physiological Relevance

Some work has been done in attempt to characterize the local inhibitory circuits responsible for this widespread inhibition via somatic whole cell recordings of pyramidal (principle) cells in piriform cortex [2]. Two temporally distinct inhibitory responses due to LOT stimulation have been revealed: early-transient inhibition and late-onset inhibition (Figure 2). These two “epochs” of inhibition onto pyramidal cells have differences in both temporal latencies and shape. Whole-cell recordings in slice has indicated early-transient inhibition is due to feed-forward inhibition by layer 1 (L1) dendrite targeting inhibitory interneurons that receive direct activation from the LOT. Whereas late-onset IPSCs are due to feed-back inhibition by layer 3 (L3) inhibitory interneurons excited by L3 pyramidal cells. This is intuitive because the dendritic filtering by L1 interneuron synapses onto pyramidal cell dendrites would cause dendritic filtering by the time these signals reached the soma, which is reflected in the more broad shape of the early transient inhibition for of inhibition observed [3]. Conversely, direct contact of L3 synapses onto the pyramidal cell soma would be sharper.

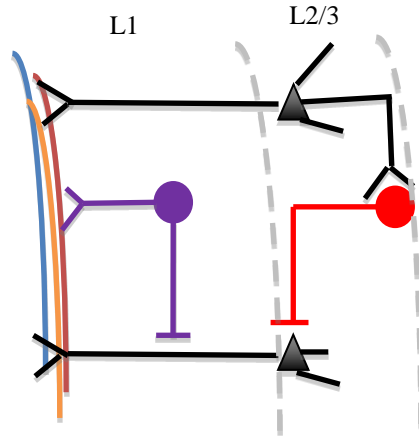


Figure 2: A circuit diagram of piriform cortex. Pyramidal cells shown in black, L1 interneurons shown in red, L3 interneurons shown in purple.

Our project will focus on modeling a class of inhibitory interneuron cell types of L3 in piriform cortex, and their contribution to the late-onset inhibition onto excitatory pyramidal cells. Functionally, this sparse activity serves to either facilitate or depress phase locking of pyramidal cell output to the respiratory cycle. For this purpose it becomes interesting to investigate the surrounding inhibitory cell populations, to determine the approximate timescales of inhibition different cell types contribute onto pyramidal cells. From this we can begin to understand mechanisms employed by inhibitory networks to shape excitatory output.

### 1.3 Goals

We have chosen to model L3 pyramidal cells because physiology and anatomy data from previously described experiments indicate similarities to two well characterized interneuron subtypes found in L3 of the piriform cortex: somatostatin (SOM) low-threshold spiking interneurons, and parvalbumin (PV) fast-spiking interneurons [4]. These interneuron subtypes are found in all sensory cortices, as well as in the hippocampus. For this project we have focused on the PV interneurons of L3 to model and implement into our network. Fortunately, between most sensory cortices (including the hippocampus), PV cell types have stereotypic behaviors which have earned them names such as “fast-spiking” parvalbumin cells. We are exploring the possibility of modeling some L1 interneurons, but there are far less candidate populations that have been as well characterized as SOM and PV cells [5].

## 2 Multi-compartment Minimal Hodgkin-Huxley Models

### 2.1 Minimal Hodgkin-Huxley Models

Pospischil et al. [6] compiled the minimal Hodgkin-Huxley (HH) models to fit experimental data from four prominent classes of neurons: fast spiking, regular spiking, intrinsically bursting, and low-threshold spiking. They found the minimal number of voltage-dependent currents with which each model could be easily fit to data from *in vivo* and *in vitro* preparations from rat, guinea pig, ferret, and cat thalamic and cortical neurons.

All models were described by the following equation:

$$C_m \frac{dV}{dt} = -I_{leak} - I_{Na} - I_{kd} - I_M - I_L$$

where  $V$  is the membrane potential,  $C_m = 1 \mu\text{F}/\text{cm}^2$  is the membrane capacitance, and  $I_{leak}$  is the passive current described by:  $I_{leak} = g_{leak} (V - E_{leak})$ , where  $g_{leak}$  is the resting membrane conductance and  $E_{leak}$  is the resting membrane potential.

The voltage-gated sodium current,  $I_{Na}$ , delayed-rectifier potassium current,  $I_{kd}$ , slow potassium current,  $I_M$ , and high-threshold calcium current,  $I_L$ , are described below.

Generally, the voltage-gated currents are described by the following equation:

$$I_j = \bar{g}_j m^M h^N (V - E_j)$$

The sodium and delayed-rectifier potassium currents ( $I_{Na}$  and  $I_{kd}$ , respectively) generate action potentials. Both models were taken from a modified HH model of central neurons by Traub & Miles [7]:

$$\begin{aligned} I_{Na} &= \bar{g}_{Na} m^3 h (V - E_{Na}) \\ \frac{dm}{dt} &= \alpha_m(V)(1-m) - \beta_m(V)m \\ \frac{dh}{dt} &= \alpha_h(V)(1-h) - \beta_h(V)h \\ \alpha_m &= \frac{-0.32(V - V_T - 13)}{\exp[-(V - V_T - 13)/4] - 1} \\ \beta_m &= \frac{0.28(V - V_T - 40)}{\exp[-(V - V_T - 40)/5] - 1} \\ \alpha_h &= 0.028 \exp[-(V - V_T - 17)/18] \\ \beta_h &= \frac{4}{1 + \exp[-(V - V_T - 40)/5]} \end{aligned} \quad \begin{aligned} I_{kd} &= \bar{g}_{kd} n^4 (V - E_K) \\ \frac{dn}{dt} &= \alpha_n(V)(1-n) - \beta_n(V)n \\ \frac{dh}{dt} &= \alpha_h(V)(1-h) - \beta_h(V)h \\ \alpha_n &= \frac{-0.032(V - V_T - 15)}{\exp[-(V - V_T - 15)/5] - 1} \\ \beta_n &= 0.5 \exp[-(V - V_T - 10)/40] \end{aligned}$$

The slow non-inactivating potassium current,  $I_M$ , is responsible for spike-frequency adaptation. The model was described by Yamada et al. [8]:

$$\begin{aligned} I_M &= \bar{g}_M p (V - E_K) \\ \frac{dp}{dt} &= (p_\infty(V) - p) / \tau_p(V) \\ p_\infty(V) &= \frac{1}{1 + \exp[-(V + 35)/10]} \\ \tau_p(V) &= \frac{\tau_{\max}}{3.3 \exp[(V + 35)/20] + \exp[-(V + 35)/20]} \end{aligned}$$

The high-threshold calcium current, which accounts for bursting, was described by Reuveni et al. [9]:

$$\begin{aligned}
I_L &= \bar{g}_L q^2 r (V - E_{Ca}) \\
\frac{dq}{dt} &= \alpha_q(V)(1-q) - \beta_q(V)q \\
\frac{dr}{dt} &= \alpha_r(V)(1-r) - \beta_r(V)r \\
\alpha_q &= \frac{0.055(-27-V)}{\exp[-(-27-V)/3.8]-1} \\
\beta_q &= 0.94 \exp[(-75-V)/17] \\
\alpha_r &= 0.000457 \exp[(-13-V)/50] \\
\beta_r &= \frac{0.0065}{\exp[(-15-V)/28]+1}
\end{aligned}$$

where  $g_L$  is the maximum conductance of the  $I_L$  current and  $E_{Ca} = 120$  mV is the reversal potential for calcium ions.

The intrinsically bursting cell was described as follows:

$$C_m \frac{dV}{dt} = -I_{leak} - I_{Na} - I_{Kd} - I_M - I_L$$

The fast-spiking interneuron was described with only spike generating currents ( $I_{Na}$  and  $I_{Kd}$ ):

$$C_m \frac{dV}{dt} = -I_{leak} - I_{Na} - I_{Kd}$$

## 2.2 Anatomical Compartmentalization

One of the key questions we wanted to address in our model was whether or not PV and SOM interneurons were physiologically capable of producing the late-onset inhibition previously described and a major component of this capability is the structure of the dendritic tree that these signals propagate through. However, to accurately approximate the anatomy of these neurons would require large amounts of experimental data. To this end we made simplified compartmentalized models that would account for average distances signals travel within a dendrite. Using these distance approximations we hoped to give more realistic temporal resolutions to our models.

Briefly, we aimed to create a concise version of our previously described circuit, with the least number of connections and compartments. To this end, we created the small network seen in Figure 4.

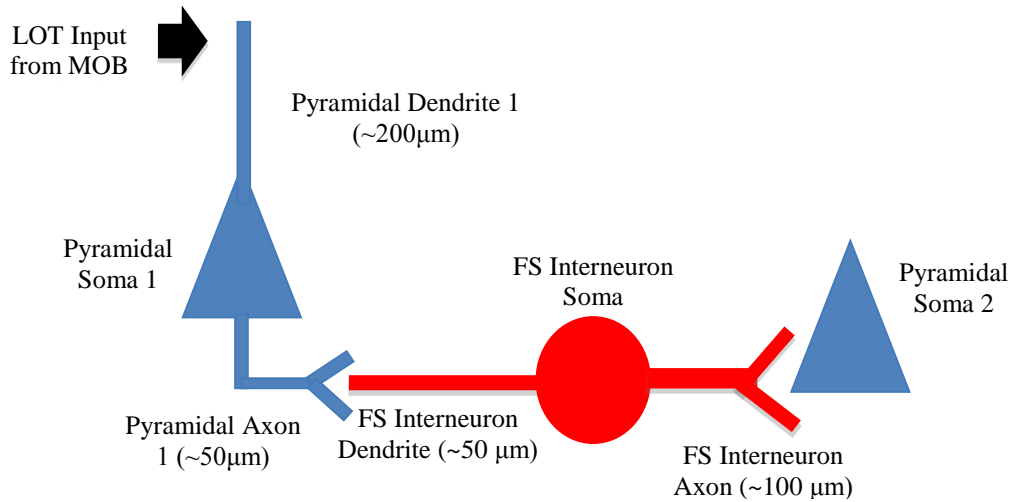


Figure 3: Schematic description of our multi-compartmental models. Distances used were approximated based on a sampling of anatomical data taken from several publications.

As seen in Figure 3 the compact nature of our circuit necessitates only 7 compartments: three somas, two dendrites and two axons. We use (this reference) for approximate soma sizes and conventional standards of dendrite and axon sizes for the remaining compartments.

### 2.3 Fitting to Experimental Data

We utilized experimentally collected whole-cell recordings of piriform cortex PV and pyramidal cell interneurons to fit our minimal Hodgkin-Huxley models. With small variations in reversal potentials and channel conductances we were able to model both neuron types with reasonable accuracy. Figure 4 shows voltage traces from whole cell recordings and our minimum Hodgkin-Huxley models. Additionally we show the stimulating voltage needed for each of our models.

We report that our models are good approximations of pyramidal and fast-spiking interneurons as assessed by their spike-rate: 19Hz experimental vs 19Hz modeled for the pyramidal neuron, and 62Hz experimental vs 64Hz modeled for the fast-spiking interneuron. We also note that the input currents necessary to get these cells to spike were similar (rheobase).

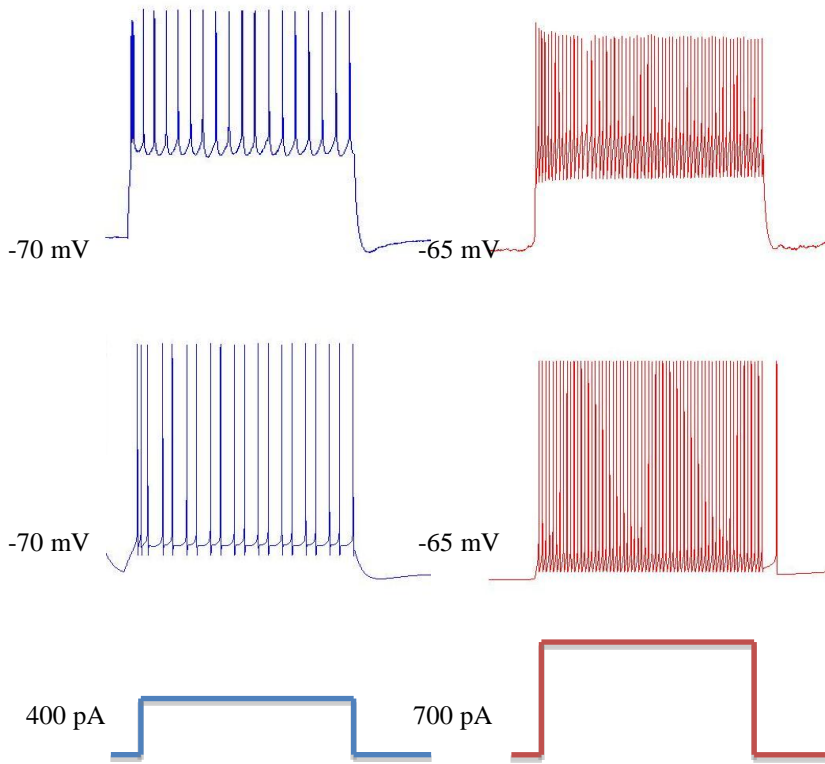


Figure 4: Experimental (top) and modeled (middle) voltage traces from piriform cortex pyramidal cells (in blue) and fast-spiking interneurons (in red) following given input currents (shown as step functions at bottom)

### 3 Connecting Models into Small Circuits

#### 3.1 Glutamate and GABA<sub>A</sub> Synapses

A glutamatic current,  $I_{Glu}$ , was used to model the excitation of the pyramidal cell onto the interneuron. A simple GABA<sub>A</sub> current,  $I_{GABA_A}$ , was used to model the inhibitory contact from the interneuron onto the second pyramidal cell.

To model the synapses, we used the following equations:

$$I_{GABA_A} = g_{GABA_A} r_i (V_{post} - E_{Cl})$$

$$I_{Glu} = g_{Glu} r_e (V_{post} - E_{Glu})$$

$$\frac{dr}{dt} = \alpha_r [T] (1 - r) - \beta r$$

$$[T] = \frac{[T]_{max}}{1 + \exp(-(V_{pre} - V_p)/K_p)}$$

where  $g_{GABA_A}$  is the peak GABA<sub>A</sub> synaptic conductance, and  $g_{Glu}$  is the peak glutamatic synaptic conductance [T] is the concentration of neurotransmitter,  $V_{pre}$  is the membrane potential of post-synaptic cell,  $V_{post}$  is the membrane potential of the post-synaptic cell,  $K_p$  is the steepness, and  $V_p$  is the value at which the function is half-activated.

### 3.2 Modeled Feed-Back Circuit

From these models we were able to insert the previously described AMPA and GABA<sub>A</sub> synapses to connect our neurons as seen in Figure 3. In Figure 5 we show this network fully initialized with pyramidal cell 1 in red, fast-spiking interneuron in green, and pyramidal cell 2 in blue. In this figure, pyramidal cell 2 has a strange voltage trace to it. This is because we chose to make pyramidal cell 2 a purely passive point process. Because the only result we wanted to see onto this neuron was the latency of the inhibition contributed by our fast-spiking neuron, we reasoned that it was not necessary to include any membrane dynamics within this cell.

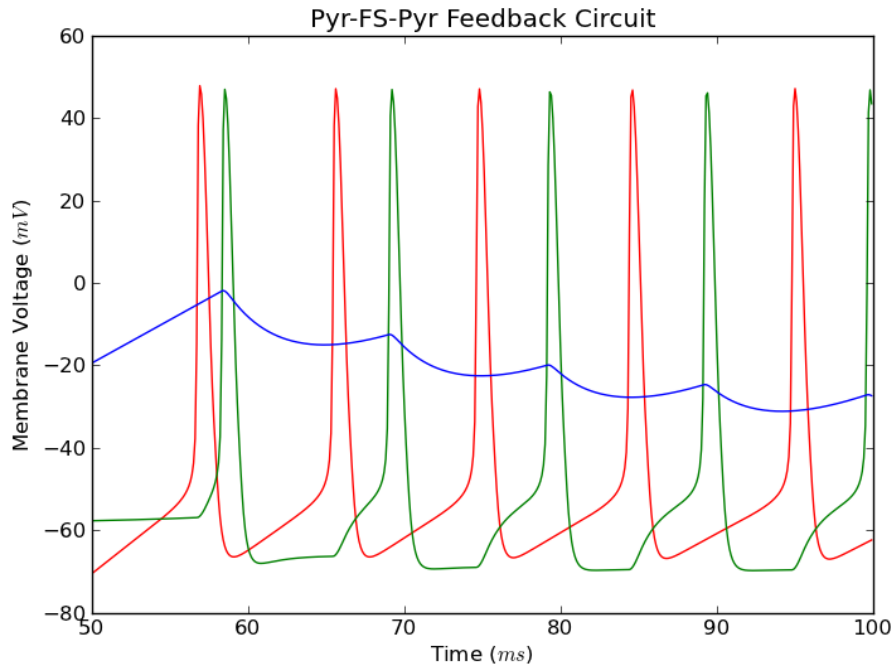


Figure 5: Voltage traces from three connected cells. The red trace represents pyramidal cell 1, the green trace represents the fast-spiking interneuron, and the blue trace represents pyramidal cell 2.

As seen in Figure 5, you can clearly see a inhibitory post-synaptic potential in pyramidal cell 2 (blue voltage trace) due to spiking in the fast-spiking inhibitory neuron. To see this more clearly, one can look at a the traces with higher temporal resolution, as seen in Figure 6.

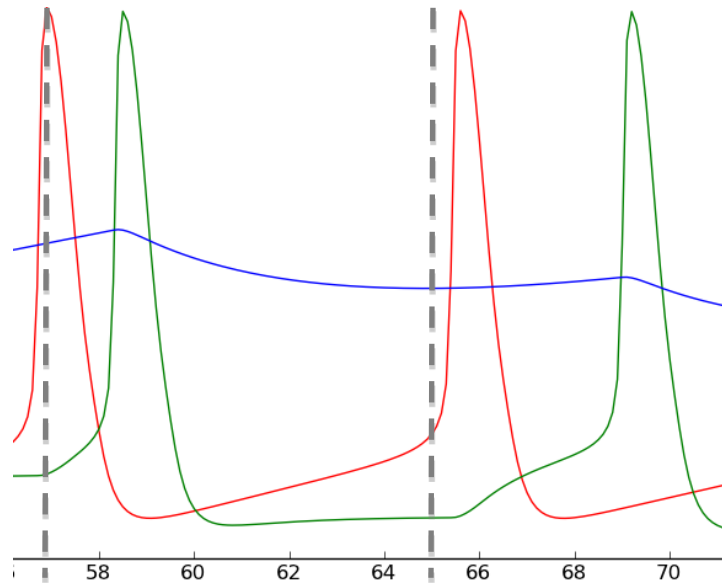


Figure 6: Higher temporal resolution of our network model seen in Figure 5. Pyramidal cell 1 in red, fast-spiking interneuron in green, pyramidal cell 2 in green. Total duration of sweep is approximately 18ms.

In Figure 6 we see that latency between pyramidal neuron 1's spike output and inhibition onto pyramidal neuron 2 is about 8 seconds (as denoted by the dashed grey lines in Figure 6). This confirms our suspicions that parvalbumin neurons may contribute to the global late-onset inhibition previously observed *in vivo*.

## 4 Conclusion

Here we showed that we were successfully able to model the pyramidal and fast-spiking neuronal cell types previously proposed. We show striking similarities between our models and previously published models from other sensory cortices. In addition we were able to create functional synaptic connections between our models. This successfully simulated one of the many piriform cortex microcircuits created by pyramidal cells and inhibitory interneurons.

It should be noted, that while we chose to focus on one interneuron cell type, there are a plethora of other interneuron types found in piriform cortex expressing different calcium binding proteins (such as: parvalbumin, calbindin, calretinin) as well as interneuron subtypes expressing different neuropeptides (such as: somatostatin, cholecystokinin, neuropeptide Y and vasoactive intestinal peptide).

## Acknowledgments

We would like to thank the extraordinary teaching assistant Mr. Jeff Bush for help implementing our model and for kind encouragement and moral support throughout our years on this planet.

## References

- [1] C. Poo and J. S. Isaacson, "Odor representations in olfactory cortex: 'sparse' coding, global inhibition, and oscillations.," *Neuron*, vol. 62, no. 6, pp. 850-61, Jun. 2009.
- [2] C. C. a Stokes and J. S. Isaacson, "From dendrite to soma: dynamic routing of inhibition by complementary interneuron microcircuits in olfactory cortex.," *Neuron*, vol. 67, no. 3, pp. 452-65, Aug. 2010.
- [3] N. Spruston, "Pyramidal neurons: dendritic structure and synaptic integration.," *Nature Reviews Neuroscience*, vol. 9, no. 3, pp. 206-21, 2008.
- [4] J. S. Isaacson and M. Scanziani, "How Inhibition Shapes Cortical Activity," *Neuron*, vol. 72, no. 2, pp. 231-243, 2011.
- [5] N. Suzuki and J. M. Bekkers, "Inhibitory interneurons in the piriform cortex.," *Clinical and experimental pharmacology & physiology*, vol. 34, no. 10, pp. 1064-9, Oct. 2007.
- [6] M. Pospischil et al., "Minimal Hodgkin-Huxley type models for different classes of cortical and thalamic neurons.," *Biological cybernetics*, vol. 99, no. 4-5, pp. 427-41, Nov. 2008.
- [7] R. D. Traub and R. Miles, *Neuronal Networks of the Hippocampus*. Cambridge University Press, 1991.
- [8] W. M. Yamada, C. Koch, and P. R. Adams, "Multiple Channels and Calcium dynamics," in *Methods in neuronal modelin*, 1989, pp. 97-133.
- [9] I. Reuveni, A. Friedman, Y. Amitai, and M. J. Gutnick, "Stepwise repolarization from Ca<sup>2+</sup> plateaus in neocortical pyramidal cells: evidence for nonhomogeneous distribution of HVA Ca<sup>2+</sup> channels in dendrites.," *Journal of Neuroscience*, vol. 13, no. 11, pp. 4609-4621, 1993.